Virtual intermediates in photosynthetic electron transfer

Julian S. Joseph* and William Bialek‡§

*Graduate Group in Biophysics, and ‡Departments of Physics and Molecular and Cell Biology, University of California at Berkeley, Berkeley, California 94720; and §NEC Research Institute, Princeton, New Jersey 08540

ABSTRACT We explore the possibility of virtual transfer in the primary charge separation of photosynthetic bacteria within the context of several types of experimental data. We show that the peak that might be expected in the virtual rate as electric fields vary the intermediate state energy is severely broadened by coupling to high-frequency modes. The Stark absorption kinetics data are thus consistent with virtual transfer in the primary charge separation. High-frequency coupling also makes the temperature dependence weak over a wide range of parameters. We demonstrate that Stark fluorescence anisotropy data, usually taken as evidence of virtual transfer, can in fact be consistent with two-step transfer. We suggest a two-pulse excitation experiment to quantify the contributions from two-step and virtual transfer. We show that virtual absorption into a charge transfer state can make a substantial contribution to the Stark absorption spectrum in a way that is not related to any derivative of the absorption spectrum.

INTRODUCTION

There has been much discussion recently concerning the role of virtual intermediates in the photosynthetic electron transfer reactions of purple bacteria. In the case of the long-range charge recombination $P^+HQ_A^- \rightarrow PHQ_A$, several authors (1–3) have noted the consistency of the observed rate and the virtual transfer rate through $P^+H^-Q_A$ estimated from the rates of $P^+H^-Q_A \rightarrow PHQ_A$ and $P^+H^-Q_A \rightarrow P^+HQ_A^-$. One of the most pressing questions surrounding the primary charge separation is whether it occurs predominantly by a two-step process or by virtual transfer (often termed a "superexchange process"). The early monomer band kinetics data (4–6) and the fluorescence anisotropy data (7) point toward virtual transfer, while more recent absorption kinetics data (8, 9) (but not reference 10) seem to suggest a two-step process. In a two-step picture the first step occurs with a rate equal to the observed $4 \times 10^{11}\ s^{-1}$, and taking $k_{23} \sim 30k_{12}$ (11) yields a reaction time for the second step of $\sim$100 fs. Vibrational relaxation in P^+B^- is likely to compete with such a fast second step, implying that the second step is nonexponential. This does not in and of itself rule out a two-step picture, however, since the second step need not have a well-defined rate constant; its nonexponential character will go unnoticed if it occurs on time scales much faster than k_{12}. It is important to emphasize that virtual transfer can occur even if the virtual intermediate state is energetically between the initial and final states.

In virtual transfer, the phase of the wave function is not randomized while the system passes through the intermediate state. We have previously shown that the detection of bleaching in the monomer band can be consistent with virtual transfer (12). After introducing a class of models, we now consider the effects of coupling to high-frequency modes, finding that weak dependence of the rate on electric fields and temperature can also be consistent with virtual transfer. However, we also show that the Stark fluorescence anisotropy data can be consistent with two-step transfer. In the hopes of resolving this issue, we suggest a two-pulse excitation experiment to distinguish between these two mechanisms. Progress toward the resolution of this issue could also be made by obtaining an experimental estimate of the electronic matrix element for the first charge transfer transition. We suggest that absorption directly into P^+B^- through P^* as a virtual intermediate is likely to make a significant contribution to the Stark absorption spectrum that, although not related to any derivatives of the absorption spectrum, is related to model parameters and could in principle be extracted. We conclude with a summary of these results.

THE CLASS OF MODELS

We work with models of three electronic states, each providing a potential for the nuclear degrees of freedom; this class of models is defined by the Hamiltonian

$$H = H_0 + H', \tag{1}$$

with

$$H_0 = \sum_{i=1}^{3} |i\rangle\langle i| H_i(y_\alpha, p_\alpha) \tag{2}$$

and

$$H' = V_{12}|1\rangle\langle 2| + V_{23}|2\rangle\langle 3| + \text{hermitian conjugate}, \tag{3}$$

where the $|i\rangle$ are three electronic states and y_α and p_α are vibrational coordinates and momenta, respectively. We take the direct matrix element $V_{13} = 0$ for convenience, although it can be included in a straightforward manner by the same methods. Treating the electronic matrix elements perturbatively and within the Condon approxi-

Dr. Joseph's present address is Laboratory of Sensorimotor Research, National Eye Institute, NIH, Bethesda, MD 20892.

0006-3495/92/08/397/15 $2.00

mation (assumed to be independent of vibrational coordinates and momenta), the virtual rate from state $|1\rangle$ (initial state) to state $|3\rangle$ (final state) is (13, Joseph and Bialek, submitted for publication)

$$k_{13} = \int_{-\infty}^{\infty} d\tau \int_0^{\infty} ds_1 \int_0^{\infty} ds_2 C(\tau - s_1, \tau, s_2, 0), \quad (4)$$

where

$$C(\tau_1, \tau_2, \tau_3, \tau_4) \equiv \langle H_{12}(\tau_1)H_{23}(\tau_2)H_{32}(\tau_3)H_{21}(\tau_4)\rangle_1 - \langle H_{12}(\tau_1)H_{21}(\tau_4)\rangle_1 \langle H_{23}(\tau_2)H_{32}(\tau_3)\rangle_2 \quad (5)$$

and the time-dependent operators are in the interaction picture with initial values of $H_{ij}(0) = V_{ij}|i\rangle\langle j|$. The angle brackets with subscripts denote thermal averages over (y_α, p_α) in the indicated electronic states. This assumes that the rate of thermal equilibration in the initial state is fast compared with the virtual rate itself.[1] We have also assumed that the second rate k_{23} of the concurrent two-step process is slow compared with the equilibration rate in the intermediate state.

Specializing to the case of harmonic modes Q_r linearly coupled to the electronic transitions and damped by a large collection of harmonic oscillators X_l, the Hamiltonian becomes

$$H = H_0 + H' \quad (6)$$

$$H_0 = \sum_{r=1}^{N} \frac{P_r^2}{2} + \sum_{i=1}^{3} |i\rangle\langle i| V_i(Q_1, \ldots, Q_N) + H_{\text{damping}} \quad (7)$$

$$V_i(Q_1, \ldots, Q_N) = \epsilon_i + \frac{1}{2}\sum_{r=1}^{N} \omega_r^2(Q_r - \bar{q}_{ir})^2 \quad (8)$$

$$H_{\text{damping}} = \sum_l \frac{P_l^2}{2} + \frac{1}{2}\sum_l \omega_l^2\left(X_l - \sum_{r=1}^{N} C_{lr}Q_r\right)^2 \quad (9)$$

$$H' = V_{12}|1\rangle\langle 2| + V_{23}|2\rangle\langle 3| + \text{hermitian conjugate.} \quad (10)$$

In this case the virtual rate is

$$k_{13} = (V_{12}V_{23}/\hbar^2)^2 \int_{-\infty}^{\infty} d\tau \int_0^{\infty} ds_1 \int_0^{\infty} ds_2 \times \exp[f_A(\tau, s_1, s_2)/\hbar]\{\exp[f_B(\tau, s_1, s_2)/\hbar] - 1\} \quad (11)$$

where

$$f_A(\tau, s_1, s_2) = i\epsilon_{13}\tau + i\epsilon_{12}(s_2 - s_1) + \sum_{r=1}^{N} q_{r,12}^2[K_r(\tau - s_1 + s_2) - K_r(0)] + \sum_{r=1}^{N} q_{r,23}^2[K_r(\tau) - K_r(0)] \quad (12)$$

$$f_B(\tau, s_1, s_2) = \sum_{r=1}^{N} q_{r,12}q_{r,23} \times [K_r(\tau - s_1) - K_r(-s_1) + K_r(\tau + s_2) - K_r(s_2)] \quad (13)$$

and $\epsilon_{ij} = \epsilon_i - \epsilon_j$, $q_{r,ij} - \bar{q}_{ir} - \bar{q}_{jr}$. The coupling to a bath of harmonic oscillators results in linear frequency-dependent damping $\gamma_r(\Omega)$. While we know that $\gamma_r(\Omega) \to 0$ as $\Omega \to \infty$, we will assume that this function is approximately flat up to a frequency ω_c that is much higher than any other frequency in the problem. We work within this "ohmic limit" because it is the simplest form of dissipation. Assuming underdamped modes, we then have

$$K_r(\tau) = \frac{\omega_r}{2}[e^{-i\omega_r\tau}(\bar{n}_r + 1) + e^{i\omega_r\tau}\bar{n}_r]e^{-\gamma_r|\tau|}, \quad (14)$$

where ω_r is the frequency[2], $\bar{n}_r = (e^{\hbar\omega_r/k_BT} - 1)^{-1}$ is the thermal mean number of phonons in the rth mode, T is the temperature, and γ_r is the damping coefficient of the rth mode.

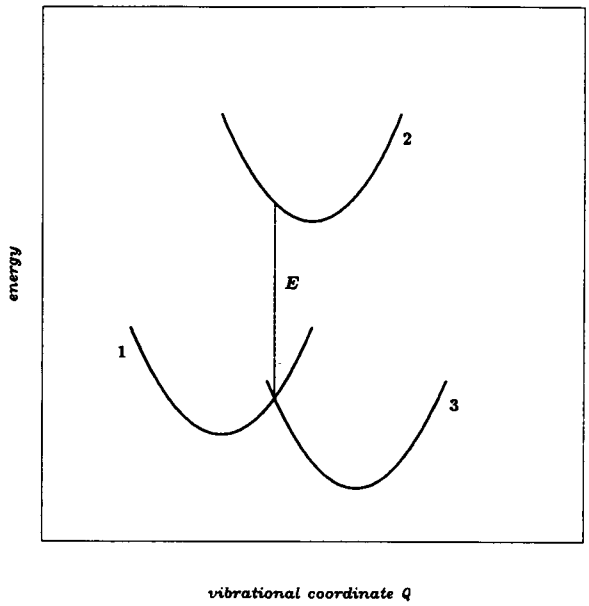

FIGURE 1 The three-state problem, showing the semi-classical energy denominator E.

Semi-classical expansions of the virtual rate can be performed for large and small values of the semi-classical energy denominator E. This quantity is defined geometrically in the case of one mode in Fig. 1. In the case of two or more modes, E is defined by the expansions. The semi-classical expansions use the saddle point approximation (or method of steepest descent) and assume the saddle points are narrow compared with their separation. To further simplify the calculations leading to the following results, we assume $\hbar\omega_r \ll \sum_{p=1}^{N} \gamma_p(\bar{n}_p + \frac{1}{2})(\frac{1}{2}q_{p,12}^2\omega_p/\hbar)$, and similarly for $q_{p,23}$. Here $q_{r,ij} = \bar{q}_{ir} - \bar{q}_{jr}$.

For a high-energy intermediate state with large E, the virtual rate is that of a two-state problem involving only the initial and final states, coupled by an effective matrix

[1] Recent experiments cast doubt on this assumption. See reference 15.

[2] Because of the damping, the oscillation frequency of the correlation function $K_r(\tau)$ is different from the parameter ω_r appearing in the Hamiltonian. From here on, ω_r will refer to the oscillation frequency.

element $V_{12}V_{23}/E$(2, 13, 16, 17). As we lower the intermediate state, this description becomes invalid when E becomes smaller than an energy on the order of $\hbar/\tau_{FC12} = [\sum_{r=1}^{N} \lambda_{r,12}\hbar\omega_r(\bar{n}+\frac{1}{2})]^{1/2}$. Here $\lambda_{r,ij} = \frac{1}{2}q_{r,ij}^2\omega_r^2$ is the contribution from the rth mode to the reorganization energy of the transition from state i to state j. The "Franck-Condon time" τ_{FC12} is interpreted as the time for two wavepackets moving separately on surfaces 1 and 2 to lose overlap with each other.

At small E, we assume that two or more modes are coupled to the transitions, and that they have comparable frequencies ω and damping coefficients γ. Upon expanding the exponent of the rate integrand about the saddle point in this case, we find a null eigenvector, forcing us to go beyond quadratic terms. For activationless reactions, this gives (13, 14)

$$k_{13} \simeq \frac{V_{12}^2 V_{23}^2}{\hbar} b_0[1 + b_2E^2] \tag{15}$$

to $\mathcal{O}(E^2)$, where

$$b_0 = N_s \frac{2\pi}{\hbar^3\Lambda^2} u^{-1/4}, \tag{16}$$

$$N_s = \coth(\pi\gamma/\omega), \tag{17}$$

$$\Lambda^4 = \frac{1}{\hbar^2}\left\{\left[\sum_{r=1}^{N} q_{r,12}^2 K_r''(0)\right]\left[\sum_{r=1}^{N} q_{r,13}^2 K_r''(0)\right] - \left[\sum_{r=1}^{N} q_{r,12}q_{r,13}K_r''(0)\right]^2\right\}, \tag{18}$$

$$u = \frac{\left[\sum_{r=1}^{N} q_{r,12}q_{r,23}K_r'''(0)\right]^2\left[\sum_{r=1}^{N} q_{r,12}^2 K_r''(0)\right]}{2\hbar^3\Lambda^4}, \tag{19}$$

and

$$b_2 = -\left\{1 + \frac{1}{\hbar^2\Lambda^4}\left[\sum_{r=1}^{N} q_{r,12}^2 K_r''(0)\right]\left[\sum_{r=1}^{N} q_{r,13}^2 K_r''(0)\right]\right\} \Bigg/ \left[-4\hbar \sum_{r=1}^{N} q_{r,12}^2 K_r''(0)\right]. \tag{20}$$

The magnitude of the rate at $E = 0$ has a complicated form because of the null eigenvector. At low temperatures, it is on the order of $k_{13}\ (E = 0) \sim (V_{12}^2V_{23}^2/\hbar^4)N_s\tau_{FC}^3S^{1/4}$, where the coupling constant is on the order $S \sim \lambda/\hbar\omega$. In most problems of interest, $S^{1/4} \sim 1$, and we may interpret this expression as having an effective energy denominator $\hbar/\tau_{FC}$. This means that the mixing of amplitude from one state into another is limited by the time scale τ_{FC}, which is just the time two wavepackets on different energy surfaces have to overlap. As E is varied from $E = 0$, the rate falls off at an energy comparable to $\hbar/\tau_{FC12}$. This is physically reasonable, since we may think of $\hbar/E$ as the time the system is allowed to spend in the virtual intermediate state by the uncertainty principle. The rate falls appreciably when this time becomes shorter than the time two wavepackets have to overlap with each other, τ_{FC12}. The factor N_s arises due to the contributions of that many saddle points. After a wavepacket is transferred to the intermediate state surface, it passes through the intermediate/final state crossing roughly N_s times before equilibration occurs in the intermediate state. Population is transferred to the final state on each pass, contributing to the rate k_{13}.

The rate as a function of the intermediate state energy can be fit by a gaussian with the correct small E behavior. The virtual rate at large E is then *under*estimated by such a fit, since in that limit it falls off only as $\sim 1/E^2$. Fig. 2 *a* shows a plot of the gaussian approximation to the virtual rate as a function of the energy of the intermediate state in one example. We see that the rate remains finite as the energy denominator vanishes, but it can display a rather pronounced peak or resonance. By experimentally varying the energies of the suspected virtual intermediate and the initial and final states, one might hope to see a resonant peak in the rate constant as the energy denominator in the effective electronic matrix element vanishes. Coupling to high-frequency modes can flatten this dependence significantly.

EFFECTS OF HIGH-FREQUENCY MODES ON THE VIRTUAL RATE

There is evidence that high-frequency modes, such as carbonyl stretches or porphyrin breathing modes, are significantly coupled to at least some of the photosynthetic electron transfer reactions (18–22). "Significant coupling" means that either $S_{H12} \equiv \frac{1}{2}q_{H12}^2\omega_H/\hbar$ or $S_{H23} \equiv \frac{1}{2}q_{H23}^2\omega_H/\hbar$ is not $\ll 1$. By "high-frequency" mode we mean any vibrational motion whose quanta approach the magnitude of the reorganization energies of the reaction. These frequencies may range from $\hbar\omega_H \simeq 400\ \text{cm}^{-1}$ for some distributed porphyrin modes to almost $\hbar\omega_H \simeq 2{,}000\ \text{cm}^{-1}$ for some local stretches.

It is natural to ask if such quantum effects invalidate the approximation of the three-state system as a two-state system with an effective matrix element. In the two-state problem, the inclusion of high-frequency modes has the qualitative effect of making the rate nearly independent of both temperature and energy gap over wide ranges. In the three-state problem, these modes can also render the virtual rate only weakly dependent on the energy of the intermediate state. Strongly quantum-mechanical modes also make the weakness of the temperature dependence robust to changes in the energy gaps of the reaction.

While the semi-classical methods used to obtain the above expressions may be used to treat low- and high-frequency modes on the same footing, the qualitative effects of coupling to the strongly quantum-mechanical high-frequency modes are more easily seen by treating them differently from the more classical low-frequency modes (23, 24). We completely ignore the damping of

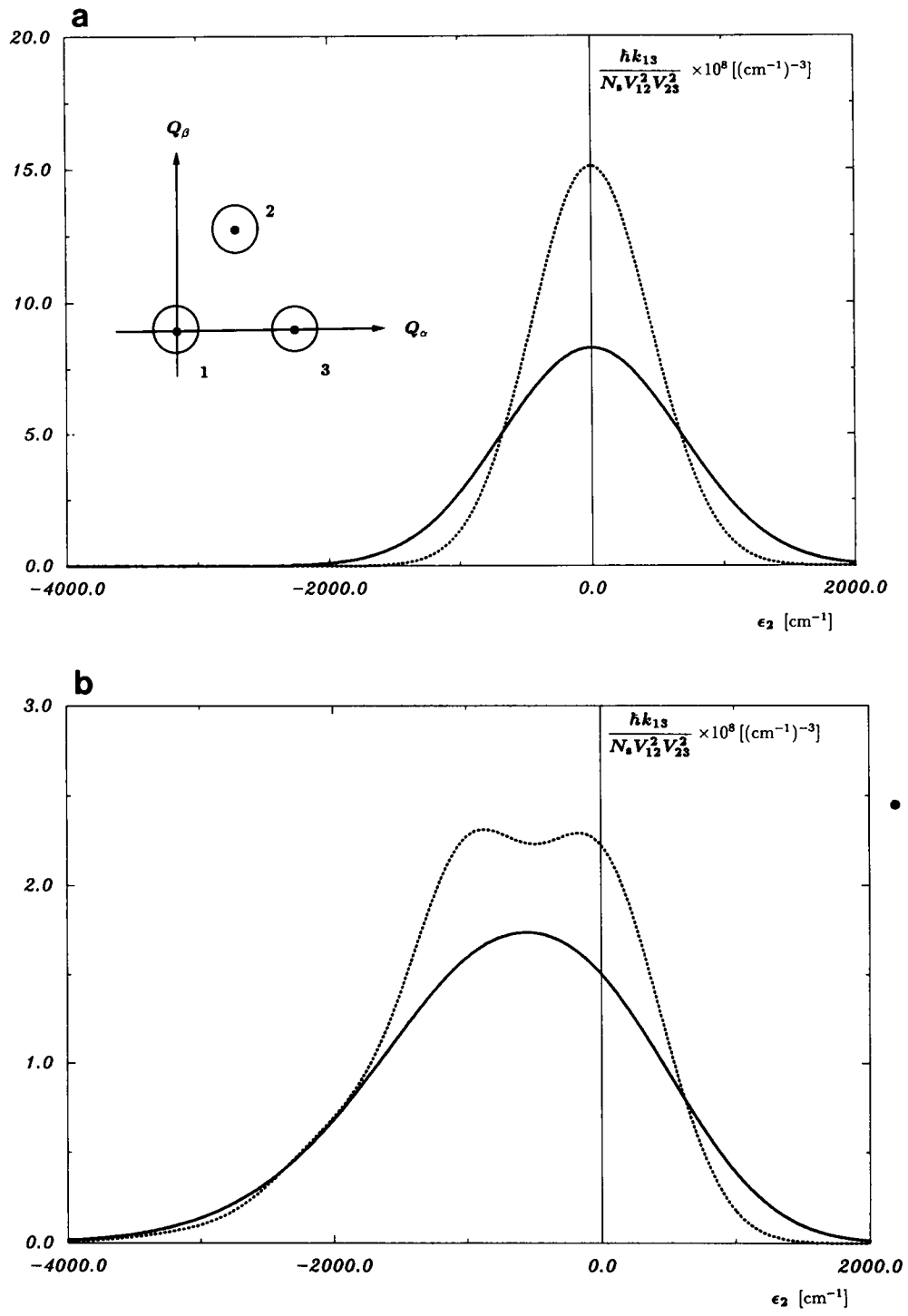

FIGURE 2 (*a*) Virtual rate versus the energy of the intermediate state in the gaussian approximation. Because the matrix elements and the factor N_s do not affect the dependence on ϵ_2, they have been factored out. For simplicity, the initial and final electronic states are held fixed in an activationless relationship while the intermediate state energy is varied. The plot shown is for the case of two modes with the equilibria of the three states arranged equilaterally, as shown in the inset. Parameters are $\epsilon_{13} = \lambda_{13} = \lambda_{12} = \lambda_{23} = 1{,}200$ cm^{-1}, $\hbar\omega_\alpha = \hbar\omega_\beta = 200$ cm^{-1}. $T = 10°$ *K* (*dotted curve*) and $T = 300°$ *K* (*solid curve*). The zero for the energy ϵ_2 is taken as the point where the semi-classical energy denominator vanishes (in this case, where $\epsilon_{12} = 1{,}200$ cm^{-1}). (*b*) Including a high-frequency mode with $\hbar\omega_H = 1{,}000$ cm^{-1}. The high-frequency reorganization parameters are $\frac{1}{2}q_{H12}^2\omega_H^2 = 1{,}000$ cm^{-1} and $q_{H23} = -q_{H12}$. The sharp peaks merge, and the rate varies by less than a factor of 3 over an energy range of 2,000 cm^{-1}. The inclusion of more high-frequency modes would make this curve even flatter. $T = 10°$ *K* (*dotted curve*) and $T = 300°$ *K* (*solid curve*).

the high-frequency modes, since these relatively localized modes probably have very long lifetimes, and simply insert complete sets of states into the correlation function appearing in the rate integral. Considering only one high-frequency mode for the sake of illustration, the rate in the two-state problem is of the form

$$k = \sum_{n=0}^{\infty} |\langle 0|\mathcal{T}(q_H)|n\rangle|^2 k_L(\epsilon - n\hbar\omega_H). \qquad (21)$$

Here $\mathcal{T}(q_H) \equiv \exp(iP_H q_H/\hbar)$ is the translation operator for the high-frequency mode, P_H is the momentum operator, q_H is the coordinate displacement between initial and final states, $\hbar\omega_H$ is the high-frequency quantum, and k_L is the rate as a function of the energy gap in the absence of high-frequency modes. The rate vs. free-energy curve of the system including the high-frequency mode is the superposition of various rate vs. free-energy curves for a system without the coupling to the high-frequency mode displaced by multiples of $\hbar\omega_H$ and weighted by the high-frequency Franck-Condon factor. If the width of each constituent curve is comparable to or larger than the high-frequency quantum, the free-energy dependence is mostly washed out over much of the inverted region. Also, any point in this region is near the peak of one of the substituent curves, so the temperature dependence is that of an activationless reaction (i.e., weak and inverted). These qualitative features are present regardless of the detailed shape of the underlying constituent curves. While coupling to modes in the intermediate range of 100–400 cm^{-1} broadens each of the constituent curves, high-frequency coupling has a more dramatic effect on the energy gap and temperature dependences. If we include several high-frequency modes instead of just one, these weak dependences become even weaker.

The three-state problem with high-frequency modes may be handled in an analogous way. Not only is the rate nearly independent of temperature and the overall energy gap over wide ranges, but it can also be nearly independent of the energy denominator over a substantial range of energies. We find the virtual rate

$$\begin{aligned} k_{13} = \int_{-\infty}^{\infty} d\tau \int_0^{\infty} ds_1 \int_0^{\infty} ds_2 \\ \times \Bigg[\sum_{m_1,m_2,n=0}^{\infty} \langle H_{12}(\tau - s_1)|m_1\rangle\langle m_1|H_{23}(\tau)|n\rangle \\ \times \langle n|H_{32}(s_2)|m_2\rangle\langle m_2|H_{21}(0)\rangle_1 \\ - \sum_{m_1,m_2=0}^{\infty} \langle H_{12}(\tau - s_1)|m_1\rangle\langle m_1|H_{21}(0)\rangle_1 \\ \times \langle H_{23}(\tau)|m_2\rangle\langle m_2|H_{32}(s_2)\rangle_2 \Bigg]. \end{aligned} \qquad (22)$$

In each thermal average, the high-frequency mode may be taken to be frozen in its ground state. This expression refers to only one high-frequency mode; several such modes may be included in precisely the same fashion. For each set of the high-frequency quantum numbers, the integral to be done involves only correlation functions of the low-frequency modes. Semi-classical saddle point methods can be applied to yield useful approximations to these integrals (13, 14). The large-E expansion has the leading term

$$\begin{aligned} k^{(0)} = (V_{12}V_{23}/\hbar)^2 \sum_{n=0}^{\infty} \tau_{FC13}(n) e^{f(\tau^*(n),0,0)/\hbar} \\ \times \left| \sum_{m=0}^{\infty} \frac{1}{E(n,m)} \langle 0|\mathcal{T}(q_{H12})|m\rangle\langle m|\mathcal{T}(q_{H23})|n\rangle \right|^2. \end{aligned} \qquad (23)$$

The various terms are weighted by the appropriate Franck-Condon factors for the high-frequency modes; $\mathcal{T}$ is the translation operator. The quantities $\tau^*(n)$ and $\tau_{FC13}(n)$ are just the saddle point location and width for a system without high-frequency modes, but with the energy of the final state raised from its actual value by $n\hbar\omega_H$. There is a different semi-classical energy denominator $E(n, m)$ for each set of high-frequency quantum numbers. This is illustrated in Fig. 3. $E(n, m)$ is just what we would find for the semi-classical energy denominator E if there were no high-frequency modes in the problem, but with the final state raised by $n\hbar\omega_H$ and with the intermediate state raised by $m\hbar\omega_H$. Note that the sum over m, the intermediate state high-frequency quantum number, is a coherent sum; i.e., the amplitudes must first be summed and then squared to yield the rate constant. The effect of high-frequency modes in modifying (or "renormalizing") the free-energy change of a two-state reaction has already been discussed. An important aspect of this (23) is that a system with $\epsilon > \lambda$ (the "inverted region") can effectively be activationless if it is coupled to high-frequency modes, because one or more terms in the sum can raise the final state enough to make the reaction activationless. In the three-state problem, we find that the emission of high-frequency quanta implies that the energy denominator does not have a unique value, and that its dominant value (the smallest) may differ significantly from the value it has before the electronic states are raised by high-frequency quanta. The most dramatic case here is one in which the dominant set of high-frequency quantum numbers causes $E(n, m)$ to be so small in magnitude that the leading term is no longer a good approximation. The rate integral is then better approximated as having a nearly vanishing semi-classical energy denominator.

We now turn to some of the experiments that attempt to vary the energies of the pertinent states in photosynthetic reaction centers of *Rhodobacter sphaeroides* and *Rhodopseudomonas viridis*. In isotropic samples, with external electric fields up to 10^6 V/cm, the fluorescence quantum yield (25) is seen to increase by a factor of only ~1.3. Furthermore, these experiments showed that the fluorescence Stark effect in quinone-containing RCs remains nearly quadratic with the electric field throughout the range of the field strength.

The dependence of the primary separation rate k

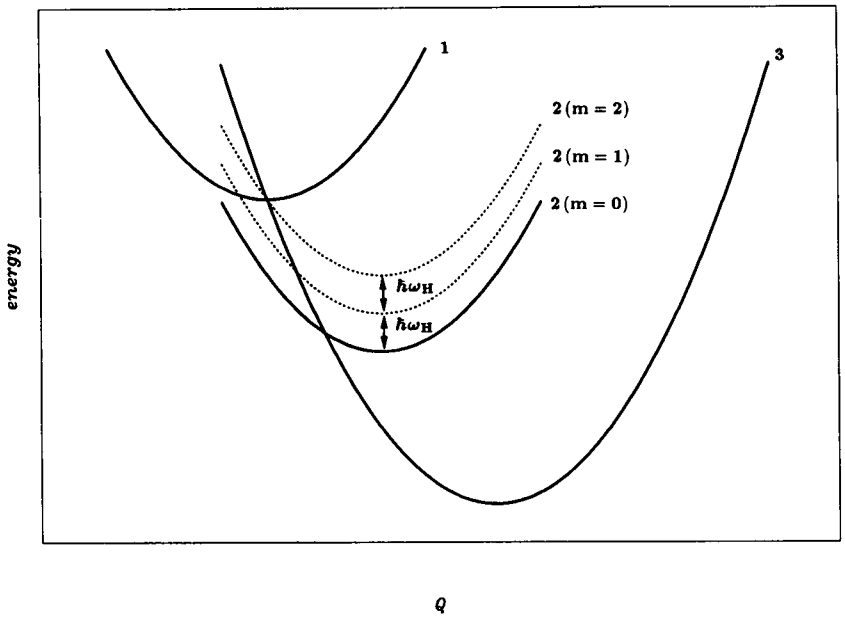

FIGURE 3 Coupling to a high-frequency mode leads to a variety of semi-classical energy denominators. The vibrational coordinate Q is a low-frequency mode. For the high-frequency quantum number $m = 0$, the energy denominator in this example is large, while for $m = 1$ it is smaller by the quantum $\hbar\omega_H$. For $m = 2$ the semi-classical energy denominator nearly vanishes.

($=k_{12} + k_{13}$) on external electric field has been extracted from absorption kinetics measurements (26). These empirical facts suggest that the primary rate varies by no more than a factor of 3 as the energy of P^+B^- varies over $\pm 1{,}000\ cm^{-1}$ and P^+H^- varies over $\pm 1{,}800\ cm^{-1}$, assuming a local field correction of 1.2 and using macrocycle center-to-center distances as estimates of the dipole moments. Theoretical estimates (27) based on virtual transfer using the large E effective matrix element, $V_{12}V_{23}/E$, and not including coupling to high-frequency modes, lead one to expect the fluorescence quantum yield to change more dramatically than is seen.

With coupling to a $1{,}000\ cm^{-1}$ mode, Fig. 2 *b* shows that varying the intermediate state energy by $2{,}000\ cm^{-1}$ changes the virtual rate k_{13} by less than a factor of 3. Emission of high-frequency quanta[3] effectively brings the state back up into a situation with $E \approx 0$. For high-frequency coupling constants close to 1, the resonance of the type shown in Fig. 2 *a* is reproduced possibly several times on one side of $E = 0$ with the spacing $\hbar\omega_H$. The vibrational structure that is present at low temperature with only one high-frequency mode in the model is blurred out if there are just a few high-frequency modes of incommensurate frequencies. Similar considerations lead to a weak dependence on the energy of the final state in the inverted region. Thus even an experiment that varies both the intermediate and final state energies, such as electric field effects, may still reveal only weak changes in the rate. We note that these qualitative features are present regardless of the detailed shape of the individual resonant peaks of Fig. 2 *a*, and regardless of their overall strength, and thus are present over a wide range of vibrational coupling parameters. This aspect of the data can be understood without detailed knowledge of the underlying parameters.

The weak energy gap dependence seen experimentally can be qualitatively understood in terms of coupling to high-frequency modes even if we suspect that the reaction proceeds by virtual transfer. Such a weak dependence of the virtual rate on the intermediate state energy may make it unnecessary to calculate the energy precisely from microscopic considerations (28), as long as the intermediate state is not more than $\sim\hbar/\tau_{FC12}$, a few hundred wavenumbers^{-1}, above P^*. If it is higher than that, we have difficulty understanding the weak field dependence. However, it can be as much as $\sim 2{,}000\ cm^{-1}$ below the initial state without showing energy dependence. This explanation of the apparent lack of field dependence rests on the state P^+B^- being either activationless or in the inverted region with respect to P^*. If this is the case, the first rate k_{12} of a two-step process is also only weakly dependent on energy gap and temperature. Thus, the weak field dependence does not in and of itself rule out virtual transfer, but it does place an upper bound on the intermediate state energy.

[3] For simplicity, only the terms with high frequency quantum numbers $m_1 = m_2$ and $n = 0$ are included here. Including other terms does not effect the curves significantly.

STARK FLUORESCENCE ANISOTROPY

Stark fluorescence anisotropy measurements were pioneered by Lockhart et al. (7, 25, 29) to determine the

initial electron acceptor. These experiments attempt to determine the angle between the transition dipole moment and the permanent dipole moment of the initial charge transfer state. This was done by applying an electric field to immobilized, randomly oriented reaction centers and measuring the polarization dependence of the change in the fluorescence intensity. The results suggest that the bacteriopheophytin is the initial acceptor, apparently providing evidence against a two-step mechanism. We argue that the possibility remains open that the primary charge separation proceeds mainly by two-step transfer, but that the Stark fluorescence anisotropy result comes about due to a small contribution from virtual transfer that has a stronger dependence on the energy gaps.

The contribution to the fluorescence intensity F from reaction centers of a particular orientation is approximately proportional to

$$F \propto (1/k)(\hat{\mathbf{e}} \cdot \hat{\mathbf{p}})^2 \tag{24}$$

where k is the rate of the primary charge separation, $\hat{\mathbf{e}}$ is the polarization vector of the fluoresced photon, and $\hat{\mathbf{p}}$ is a unit vector along the fluorescence transition dipole moment.

It was assumed in references 7, 25, and 29 that the electron transfer rate is affected by the electric field only through its dependence on the energy gap between the initial and final states. In other words, a two-state analysis was performed. The change in the fluorescence spectrum due to the electric field is mostly proportional to the 0th derivative of the spectrum, although there is also a first derivative component. By Taylor–expanding $1/k$ for sufficiently weak electric fields and averaging uniformly over the orientation (assuming the reaction centers are identical aside from orientation), one arrives at the expression for the 0th derivative component of the change in fluorescence intensity,

$$\Delta F \propto |\vec{\mu}_{et}|^2 |\vec{\mathbf{E}}|^2 \left\{ \frac{1}{9} + \frac{1}{5}\left[(\hat{\mu}_{et} \cdot \hat{\mathbf{p}})^2 - \frac{1}{3} \right]\left[(\hat{\mathbf{E}} \cdot \hat{\mathbf{e}})^2 - \frac{1}{3} \right] \right\}. \tag{25}$$

Here $\vec{\mathbf{E}}$ is the change in the internal electric field due to the externally applied electric field. This is larger than the applied field by a factor called the "local field correction" f, which has been estimated to be between 1.2 and 1.8 (30–32). We will assume that the local field correction is homogeneous and isotropic, and that polarizability differences are negligible. The last factor involves the internal electric field and the polarization of the fluoresced photon. A fit to the dependence on the angle between these vectors determines the angle between the transition dipole and the difference dipole $\vec{\mu}_{et}$. After separating out the effect of the emission difference dipole (29), the result in *Rb. sphaeroides* at 77° K was 65 ± 2°, suggesting that the bacteriopheophytin is the initial acceptor.

Now if virtual transfer ("superexchange") is suggested by this result, we must deal with the fact that the virtual rate in general depends not only on the overall energy gap of the reaction but also on the initial/intermediate energy gap. This leads us to a three-state analysis of the experiment that is independent of any model for the reaction.

We consider three electronic states, 1, 2, and 3, with the two energy gaps, ϵ_{12} and ϵ_{23}, and assume that the primary separation rate depends on no energy gaps other than ϵ_{12} and ϵ_{23}. Here $\epsilon_{ij} = \epsilon_i - \epsilon_j$. In the general situation, the electric field affects the electron transfer rate through its effect on both of these energies, so the Taylor expansion for weak fields is a bit more complicated:

$$\begin{aligned} \Delta F \propto & \frac{\partial^2(1/k)}{\partial \epsilon_{12}^2} \langle (\vec{\mu}_{12} \cdot \vec{\mathbf{E}})^2 (\hat{\mathbf{e}} \cdot \hat{\mathbf{p}})^2 \rangle \\ & + 2 \frac{\partial^2(1/k)}{\partial \epsilon_{12} \partial \epsilon_{23}} \langle (\vec{\mu}_{12} \cdot \vec{\mathbf{E}})(\vec{\mu}_{23} \cdot \vec{\mathbf{E}})(\hat{\mathbf{e}} \cdot \hat{\mathbf{p}})^2 \rangle \\ & + \frac{\partial^2(1/k)}{\partial \epsilon_{23}^2} \langle (\vec{\mu}_{23} \cdot \vec{\mathbf{E}})^2 (\hat{\mathbf{e}} \cdot \hat{\mathbf{p}})^2 \rangle. \end{aligned} \tag{26}$$

Here $\vec{\mu}_{12}$ is the difference dipole between states 1 and 2, and $\vec{\mu}_{23}$ is the difference between states 2 and 3. The angled brackets denote the orientational average. The first and last terms have the same form required for the two-state analysis; this expression has been calculated previously (33). The mixed term is shown in the Appendix to be given by[4]

$$\begin{aligned} \langle (\hat{\mu}_{12} \cdot \hat{\mathbf{E}})(\hat{\mu}_{23} \cdot \hat{\mathbf{E}})(\hat{\mathbf{e}} \cdot \hat{\mathbf{p}})^2 \rangle = & \tfrac{1}{9} \hat{\mu}_{12} \cdot \hat{\mu}_{23} \\ & + \tfrac{1}{5}[(\hat{\mu}_{12} \cdot \hat{\mathbf{p}})(\hat{\mu}_{23} \cdot \hat{\mathbf{p}}) - \tfrac{1}{3} \hat{\mu}_{12} \cdot \hat{\mu}_{23}][(\hat{\mathbf{E}} \cdot \hat{\mathbf{e}})^2 - \tfrac{1}{3}], \end{aligned} \tag{27}$$

where a $\hat{}$ denotes a unit vector.

Putting the terms together, we find that the dependence on the angle χ between the electric field and the fluorescence polarization is precisely the same as in the two-state analysis:

$$\Delta F \propto \tfrac{1}{9} + \tfrac{1}{5}[\cos^2 \zeta_{eff} - \tfrac{1}{3}][\cos^2 \chi - \tfrac{1}{3}]. \tag{28}$$

In the two-state analysis, the angle ζ_{eff} is just the angle between the transition dipole and the difference dipole moment between the initial excited state and the final state of the reaction, the first charge transfer state. In that interpretation,

[4] An average of the same form enters into an analytical disentanglement of the emission difference dipole effect (first derivative component) from the total Stark fluorescence anisotropy spectrum.

$$\cos \zeta_{eff} = \hat{\mu}_{et} \cdot \hat{\mathbf{p}}, \tag{29}$$

where $\hat{\mu}_{et}$ is a unit vector along the difference dipole moment between P^* and the primary charge transfer state. The angle ζ_{eff} was experimentally determined to be 65°.

The three-state analysis gives

$$\begin{aligned}\cos^2 \zeta_{eff} - \frac{1}{3} = \Bigg\{ & \frac{\partial^2(1/k)}{\partial \epsilon_{12}^2}\left[(\vec{\mu}_{12}\cdot\vec{\mathbf{p}})^2 - \frac{1}{3}\mu_{12}^2\right] \\ & + 2\frac{\partial^2(1/k)}{\partial \epsilon_{12}\partial \epsilon_{23}}\left[(\vec{\mu}_{12}\cdot\vec{\mathbf{p}})(\vec{\mu}_{23}\cdot\vec{\mathbf{p}}) - \frac{1}{3}\vec{\mu}_{12}\cdot\vec{\mu}_{23}\right] \\ & + \frac{\partial^2(1/k)}{\partial \epsilon_{23}^2}\left[(\vec{\mu}_{23}\cdot\vec{\mathbf{p}})^2 - \frac{1}{3}\mu_{23}^2\right]\Bigg\} \\ & \times \left[\frac{\partial^2(1/k)}{\partial \epsilon_{12}^2}\mu_{12}^2 + 2\frac{\partial^2(1/k)}{\partial \epsilon_{12}\partial \epsilon_{23}}\vec{\mu}_{12}\cdot\vec{\mu}_{23} \right. \\ & \left. + \frac{\partial^2(1/k)}{\partial \epsilon_{23}^2}\mu_{23}^2\right]^{-1}. \end{aligned} \tag{30}$$

It is important to note that these expressions for the Stark change in fluorescence and the effective angle ζ_{eff} are independent of any models that one might propose for the primary charge separation.

In contrast to the result of the two-state analysis, the effective angle ζ_{eff} depends on the second partial derivatives of the reciprocal electron transfer rate with respect to the energy gaps, or on two ratios of these three quantities. It also depends on the difference dipole moments and the angle between them. If the primary separation proceeds purely by direct transfer, then all the derivatives are equal and the expression reduces to the two-state result with $\cos \zeta_{eff} = \hat{\mu}_{13} \cdot \hat{\mathbf{p}}$. If the reaction proceeds purely by a two-step mechanism, then only the second derivative with respect to ϵ_{12} is nonzero, and the expression reduces to the two-state result with $\cos \zeta_{eff} = \hat{\mu}_{12} \cdot \hat{\mathbf{p}}$. If virtual transfer plays a role, however, or if two or more of these mechanisms contribute significantly, the observed angle is a complicated combination of various parameters of the system.

It is then natural to ask if two-step transfer might actually be dominating the reaction, while a small contribution to the rate from virtual transfer affects the experimentally observed angle ζ_{eff}. The dependence of the observed angle on the energy gap derivatives suggests that this might be possible if the virtual rate has a sufficiently strong dependence on the intermediate/final energy gap ϵ_{23}. We will make a rough order of magnitude estimate of how strong this dependence must be if it is to affect our conclusions about the mechanism.

The observed angle places a severe constraint on the dependence of the rate on the energy gaps. We consider the three states that might be involved in the initial charge transfer to be P^*, P^+B^-, and P^+H^-. We will assume the difference dipoles are given by the center-to-center distances between the macrocycles. The values we use are taken from the *Rps. viridis* structure (34, 35); the values for *Rb. sphaeroides* (36) are nearly identical. The centers of B and H are taken to be the average of the four central nitrogens; the center of the special pair is taken as the average of the centers of each of its constituent monomers. We neglect the dipole moment of P^*. Following references 7 and 37 we take $\hat{\mathbf{p}} \cdot \hat{\mu}_{21} = \cos 45.9°$ and $\hat{\mathbf{p}} \cdot \hat{\mu}_{31} = \cos 57.7°$. (Let $\vec{\mu}_{21} = \vec{\mu}_2 - \vec{\mu}_1 = -\vec{\mu}_{12}$ and similarly for the other difference dipoles.)

The Stark fluorescence data together with the above expressions then lead to the following constraint:

$$-2.2\frac{\partial^2(1/k)}{\partial \epsilon_{12}^2} - 0.8\frac{\partial^2(1/k)}{\partial \epsilon_{12}\partial \epsilon_{23}} + \frac{\partial^2(1/k)}{\partial \epsilon_{23}^2} = 0. \tag{31}$$

We now suppose that 90% of the primary separation rate is the first rate of a two-step process, which we will assume to be independent of ϵ_{23}. For the sake of our calculation we take the remaining 10% to be due to virtual transfer. The above constraint suggests that all three derivatives are of the same order of magnitude, since the coefficients are of order unity. This can be satisfied if the energy $\delta\epsilon_{23}$ over which the virtual rate varies appreciably is roughly three times smaller than the energy $\delta\epsilon_{12}$ over which the total rate undergoes significant variation. If this is the case, $\delta\epsilon_{12}$ is given by the scale of the energy gap dependence seen in Stark absorption kinetics studies (38). The experiments (38) showed the rate dropping from its peak by a factor of $e^{-1/2}$ over an energy range of $\approx$800 cm^{-1}. This curve was presented with a value of f= 1 for the local field correction. If we assume a value of 1.5, this energy scales to $\approx$1,200 cm^{-1}. We must also account for the fact that the curve in reference 38 was calculated assuming a dipole moment of 82 D for the initial charge transfer state. Since we are considering the possibility that the monomer is for the most part the initial acceptor (with a dipole moment of $\sim$50 D), we must scale the energy down by the ratio of these moments, giving $\delta\epsilon_{12} \approx$ 750 cm^{-1}. This means the virtual rate must fall significantly from its peak as we vary the energy of P^+H^- by $\sim$250 cm^{-1}. If this order of magnitude for the dependence of the virtual rate on the second energy gap is implausible, then the data implicate virtual transfer as the dominant process in the transfer.

We must ask how strong the virtual rate dependence on ϵ_{23} can plausibly be. The expressions for the virtual rate at the small energy denominator given above show that the virtual drops by $e^{-1/2}$ when the P^+B^- energy[5] is varied by $<(2\lambda_{12}\hbar\omega)^{1/2}$, where λ_{12} is the reorganization energy between P^* and P^+B^- and ω is a typical mode frequency coupled to the transition (assuming $\hbar\omega \gg$

[5] In this section we consider varying ϵ_{23} while keeping ϵ_{12} fixed, which is equivalent to varying the P^+H^- energy. This changes both the energy denominator and the activation energy. The estimate for $\delta\epsilon_{23}$ is based, however, on calculations in which the P^+B^- energy is varied, which only changes the energy denominator. We assume that the resulting energy changes are of comparable magnitude.

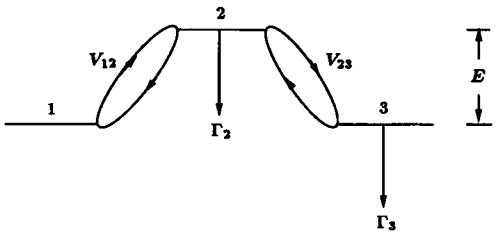

FIGURE 4 Simple picture of three states with amplitude loss. The virtual rate depends on Γ_3, while the first rate of the two-step transfer does not. In the perturbative limit, the virtual rate is proportional to $1/\Gamma_3$, regardless of the intermediate state energy.

$k_B T$). We assume that either coupling to high-frequency modes is insignificant or that ϵ_{23} is in or near the normal region. Taking $\lambda_{12} \approx 300$ cm^{-1} and $\hbar\omega \approx 200$ cm^{-1} gives[6] $\delta\epsilon_{23} \approx 350$ cm^{-1}. Although the approximations used in this order of magnitude estimate were crude, the proximity of this scale of variation to that required opens the possibility of a reinterpretation of the experimental result.

In summary, we have described a scenario, consistent with the Stark fluorescence anisotropy data, in which virtual transfer contributes only ~10% to the primary charge separation, while the apparent angle between the transition dipole and the dipole moment of the initial acceptor state is close to the observed 65°. To open this alternative interpretation, however, we had to go to the limits of physically plausible energy gap dependences.

A TWO-PULSE EXCITATION EXPERIMENT

We have seen that several experiments aimed at elucidating the mechanism of the primary charge separation are inconclusive when considered individually. Although we might hope that the body of data taken as a whole will be consistent with only one of the proposed mechanisms, the large number of parameters in the models might not allow such a firm conclusion. We now propose an experiment to distinguish between virtual and two-step transfer processes, with the aim of finding a signature that is independent of the underlying system parameters over a certain range.

The idea is motivated by the simple picture of three levels shown in Fig. 4. The virtual rate depends on Γ_3, while the first rate of the two-step process is independent of Γ_3 (12). The virtual rate is proportional to $1/\Gamma_3$, assuming the perturbative approximation V_{12}, $V_{23} \ll \Gamma_3$ and the larger of E and Γ_2. This holds regardless of the energy of the intermediate state. If we can increase Γ_3 experimentally, a decrease in the rate will indicate virtual transfer while no change is indicative of a two-step process.

[6] With these parameters values, the semi-classical approximation used to produce this expression is close to breaking down.

In Fig. 4, Γ_3 is the rate at which the coherent mixing from state 2 decays. How can we increase this experimentally? One way is to remove amplitude from the P^+H^- levels with radiative excitation in the H^- band at 665 nm.[7] The idea is to excite the system at 870 nm with a pulse of typical energy and duration, and after an appropriate amount of time excite the system with an intense pulse centered at 665 nm. During the H^- excitation, pulses probing the stimulated emission[8] should detect a slowing down of the kinetics. Our job now is to calculate the intensity and duration of the H^- pulse required to see an effect in the event of virtual transfer.

How large is Γ_3? To know how much of an effect to expect, we need an upper bound on the natural value of Γ_3. While Fig. 4 seems to suggest that Γ_3 is the dephasing rate of the participating excited P^+H^- levels, it might be even faster than that. If a vibrational wavepacket on the P^+H^- surface moves away from the P^+B^- crossing point before it dephases, but dephasing occurs before the completion of one vibrational period, the amount of mixing from P^+B^- is limited not by the dephasing rate but rather by the time to move away from the crossing point (17). At low temperatures this is given by $(\lambda\hbar\omega)^{1/2}/\hbar$, where λ is the P^+B^-/P^+H^- reorganization energy and ω is the frequency of a typical semi-classical mode coupled to the transition. For an upper bound on Γ_3, we use the reorganization energy of the overall P^*/P^+H^- reaction, assumed to be $\approx$1,200 cm^{-1}. For a semi-classical mode of relatively high frequency we use $\hbar\omega \approx 200$ cm^{-1}. This gives an upper bound of $\hbar\Gamma_3 \leq 500$ cm^{-1}, or $\Gamma_3 \leq 1 \times 10^{14}$ s^{-1}. It is important to note that while model parameters were used to obtain this upper bound, the underlying vibronic parameters need not be known to interpret the experimental results as long as we are in the perturbative regime (and in the absence of the complications noted below).

We require the H^- pulse to be intense enough to change the time constant by more than the experimental error. At 8K the time constant is 1.2 ± 0.1 ps (39). The increase $\delta\Gamma_3$ must therefore be at least

$$\delta\Gamma_3 = \Gamma_3 \frac{0.1}{1.2} \simeq 8 \times 10^{12}\ \text{s}^{-1}. \tag{32}$$

Denoting the absorption cross-section at 665 nm by σ_{665}, the required intensity by I_{665}, and the photon frequency by Ω, the rate of radiative amplitude loss is given by

$$\delta\Gamma_3 = \frac{1}{2}\frac{\sigma_{665} I_{665}}{\hbar\Omega_{665}}. \tag{33}$$

The factor of ½ is due to the fact that Γ_3 corresponds to amplitude loss, not population loss. The cross-section

[7] The numbers quoted here refer to *Rb. sphaeroides*. Analogous statements hold for *Rps. viridis*.

[8] Note that probing the appearance of the P^+ band rather than the stimulated emission could be deceiving because vibrational relaxation could cause spectral changes during the experiment.

has been measured in the *Rb. sphaeroides* (40) to be about $\sigma_{665} = 5.8 \times 10^{-17}$ cm^2. This yields a required intensity of $I_{665} = 8 \times 10^{10}$ W/cm^2.

If we are to avoid nonlinearity in the H^- absorption, we are limited in the total energy per unit area $\mathcal{E}$ of the H^- pulse. The highest we can go is given by

$$\frac{\mathcal{E}\sigma_{665}}{\hbar\Omega_{665}} \sim 1, \tag{34}$$

which limits us to $\mathcal{E} \leq 5 \times 10^{-3}$ J/cm^2. To achieve the required intensity, the pulse duration must then be no greater than $\approx$60 fs. The rate of stimulated emission decay could be probed during the H^- excitation. Because the half-width of the P band at low temperatures is $\approx$200 cm^{-1}, the probe pulse cannot be shorter than $\approx$30 fs. The best signal to noise ratio should be obtained if the H^- pulse is delivered after the initial rise in the stimulated emission, but less than one $1/e$ time thereafter.

Suppose we do see the rate decrease. It could be that virtual transfer makes only a small contribution, but that Γ_3 is smaller than we thought. To remove this ambiguity, we need a measurement at another value of $\delta\Gamma_3$, which could be obtained with 30-fs pulses in the H^- band. Such pulses have a spectral width no greater than that of the H^- band at low temperatures (41). If the pulses can be timed with sufficient accuracy, and with enough averaging, it will be possible to obtain measurements of the rate constant in the H^- excitation window. Together with the rate measurement at $\delta\Gamma_3 = 0$, we would then have three measurements available, and we could fit the rate to the functional form

$$k(\delta\Gamma_3) = \frac{a}{\Gamma_3 + \delta\Gamma_3} + b, \tag{35}$$

adjusting the parameters a, b, and Γ_3. The additive constant is the first rate of the two-step process. We can then determine whether two-step transfer dominates the decay of P^*.[9]

We anticipate certain problems with this experiment. The values of the center frequency, width, and cross-section of the H^- band we have used in these calculations are those at 20–30 ps after the initial excitation. It is conceivable that due to vibrational relaxation in P^+H^- these values are different from those relevant on the femtosecond time scale. The relevant values can in principle be determined experimentally. The intensity of the H^- excitation might cause nonlinear optical effects in the medium surrounding the reaction centers, although such effects could be characterized on blank samples. A problem that is perhaps more serious is the presence of absorption in the vicinity of 665 nm in the ground state. The transitions responsible for this absorption could complicate the interpretation of the data. If these transitions can be identified, their effect on the data could be estimated and accounted for. Manufacturing the required pulses may also pose a problem. Pulses of sufficient energy and brevity have been produced (42), but these had a center wavelength of 625 nm.

To summarize, we have suggested an experiment to distinguish two-step transfer from virtual or direct transfer in the primary charge separation. The procedure can be outlined as follows:

(*1*) Pump the system in the P band with an energy to excite <20% of the reaction centers.

(*2*) Shortly after the rise in the stimulated emission, excite the system in the H^- band with a 60-fs pulse of 5 mJ/cm^2.

(*3*) Probe the stimulated emission during the H^- excitation with 30-fs pulses.

(*4*) Repeat using a 30-fs pulse for the H^- excitation.

(*5*) Use the three available rate measurements to fit the functional form

$$k(\delta\Gamma_3) = a/(\Gamma_3 + \delta\Gamma_3) + b.$$

This determines whether the first rate of the two-step process, b, is greater than the sum of the virtual and direct rates, a/Γ_3. In the perturbative regime, one can interpret the data in this way without a detailed Hamiltonian to describe the system.

ABSORPTION THROUGH P^* AS A VIRTUAL INTERMEDIATE

Second-order perturbation theory allows some absorption from the ground state to a charge-transfer state, since the ground state is radiatively connected to P^* while P^* is connected to charge transfer states by electronic matrix elements. This has been discussed previously by several authors (43, 44). While there is the possibility of a transient intradimer charge transfer state in the wild-type (45–47) and in heterodimer mutants (48, 49), we will focus our discussion on absorption into P^+B^-. It is natural to ask if this absorption plays any functional role in facilitating charge transfer, and whether it can affect any of the experimental data used to probe the primary charge separation. To answer these questions, we need to estimate this cross-section and its dependence on the photon frequency Ω.

One way to calculate a cross-section that emphasizes the similarities to a rate calculation is to put the system in a large box of volume $\mathcal{V}$. There is one photon of frequency Ω in this box, so the photon density is $1/\mathcal{V}$ and the flux density $\mathcal{J}$ of the light impinging on the reaction center is $c/\mathcal{V}$, where c is the speed of light. We then have to calculate the rate k_ν to go from the ground state PB to the charge transfer state (P^+B^-). The cross-section for

[9] A contribution from direct transfer, mediated by direct coupling between P^* and P^+H^-, is indistinguishable from virtual transfer in this experiment.

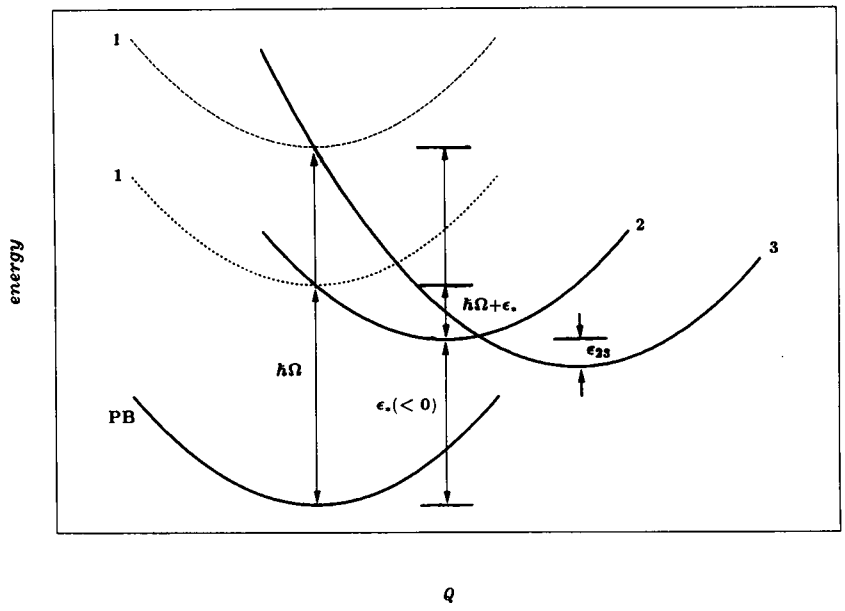

FIGURE 5 The cross-section to absorb from the ground state into P^+B^- is proportional to the rate constant to go from state 1 to state 3 virtually through state 2. The vibrational surface of state 1 is that of the ground state raised by the photon energy $\hbar\Omega$ (shown for two values of Ω), while state 2 is P^* and state 3 is P^+B^-. The figure defines the energy gaps ϵ_* and ϵ_{23} referred to in the text. The dashed curve is the state 1 surface for a photon frequency at the peak of the absorption into P^+B^-, where states 1 and 3 are in an activationless relationship; $\hbar\Omega = \lambda_{13} - \epsilon_* - \epsilon_{23}$. The dotted curve is the peak of the absorption into P^*, where states 1 and 2 are in an activationless relationship; $\hbar\Omega = \lambda_{12} - \epsilon_*$.

the absorption into P^+B^- is then $\sigma_V = k_V/\mathcal{J}$. We can calculate this rate to lowest nonvanishing order in the perturbations $-\vec{\mathbf{p}}\cdot\vec{\mathbf{E}}$ and $V(|2\rangle\langle 3| + \text{hermitian conjugate})$, where $\vec{\mathbf{p}}$ is dipole moment operator and $\vec{\mathbf{E}}$ is the electric field operator (50). We have denoted the intermediate state P^* by $|2\rangle$ and the final state P^+B^- by $|3\rangle$. The electronic matrix element coupling these states is V, which is equal to the matrix element V_{12} we referred to in the discussion of the primary charge separation. I assume that there is no transition dipole matrix element between PB and P^+B^-, and we make the Condon approximation for the transition dipole (it is independent of the vibrational coordinates and momenta). We then have a virtual rate calculation that is formally identical to the virtual electron transfer rate calculations. After the electric field acts on the photon part of the state vector, the vibrational surface of the ground state is raised by $\hbar\Omega$, and we can consider this the initial state (state 1) of the reaction. This is illustrated in Fig. 5.

At a given photon frequency, the ratio of the cross-section into P^+B^- to the cross-section into P^* is precisely equal to the ratio of the virtual rate in Fig. 5 to the first rate of the two-step process (i.e., the rate from state 1 to state 2). In general, as shown in Fig. 5, the peak frequencies of these two cross-sections are different, so the bands do not necessarily coincide. The P^+B^- cross-section has a peak at $\hbar\Omega = \lambda_{13} - \epsilon_* - \epsilon_{23}$, while the P^* cross-section has a peak at $\hbar\Omega = \lambda_{12} - \epsilon_*$. Under the same simplifying assumptions used in the electron transfer calculations, the ratio of the peak absorptions of these two bands is on the order of

$$\sigma_{V\max}/\sigma_{*\max} \sim \coth(\pi\gamma/\omega)\frac{V^2}{\lambda_{12}\hbar\omega}S^{1/4} \qquad (36)$$

at low temperatures, with the appropriate modification at high temperatures. The ratio may be smaller than this if the energy denominator at the virtual absorption peak is large. Here ω is the frequency of a typical vibrational mode with damping coefficient γ and dimensionless coupling S. We tentatively assign the half-width at half-maximum of the P band ($\approx$200 cm^{-1} at low temperatures) to the vibronic energy fluctuation $(\lambda_{12}\hbar\omega)^{1/2}$. As an estimate we also take $V \approx 20$ cm^{-1}, $\omega/(\pi\gamma) \approx 3$, and $S^{1/4} \approx 1$. With these numbers, the strength of the P^+B^- absorption band is a few percent of the P band maximum. The process may be only a slight perturbation to the ground state absorption spectrum. Nonetheless, we will see that the effect of virtual absorption on the Stark absorption spectrum can be potentially severe.

It is interesting to note that the absorption into P^+B^- may actually have two peaks, even if there is no coherent vibrational recurrence. Kharkats and co-workers (51) showed in the case of one mode with equal displacements in the transitions that the activation energy of the virtual rate is given by the energy from the equilibrium of the initial state to the higher of the initial/intermediate and intermediate/final crossings, if these are both lower than the initial/final crossing. In the example of Fig. 5, this other peak in the virtual cross-section coincides with the peak of the P band. In Fig. 6, however, we give an example in which this "Kharkats peak" is at a

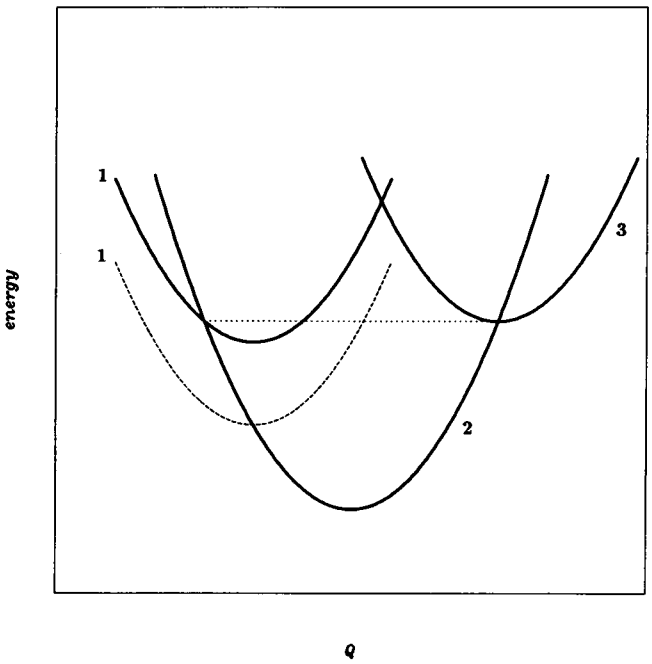

FIGURE 6 A second peak in the spectrum of virtual absorption into P^+B^- may exist. In the example shown here, this peak (solid state 1 curve) is at a higher frequency than the P band peak (dashed state 1 curve).

higher frequency than the P band. To be resolvable, this peak must be separated from all others by at least each of their widths. Unfortunately, the assumptions made in the calculations do not allow us to estimate the strength or width of this peak.

While it does not appear likely that virtual absorption into P^+B- contributes significantly to the ground state absorption spectrum, it may have a severe effect on the Stark absorption spectrum, since the dipole moment of P^+B^- could be an order of magnitude greater than the difference dipole between P and P^*. Because the Stark effect probes the nature of the initial states involved in electron transfer, we would like to understand other processes that can affect these data.

Consider a sample of immobilized and randomly oriented reaction centers subjected to an external voltage that changes the internal electric field by $\vec{\mathbf{E}}$. Let the total absorption cross-section be $\sigma = \sigma_* + \sigma_V$. Let $\tilde{\sigma} = \sigma/[\Omega(\hat{\epsilon}\cdot\hat{\mathbf{p}})^2]$, and likewise for $\tilde{\sigma}_*$ and $\tilde{\sigma}_V$. We know that $\tilde{\sigma}_*$ is a function of $\epsilon_* + \hbar\Omega$, while $\tilde{\sigma}_V$ is a function of $\epsilon_* + \hbar\Omega$ and also ϵ_{23}. The Stark absorption change is

$$\Delta\left(\frac{\sigma}{\Omega}\right) = \frac{\partial^2\tilde{\sigma}}{\hbar^2\partial\Omega^2}\langle(\hat{\epsilon}\cdot\hat{\mathbf{p}})^2(\vec{\mu}_*\cdot\vec{\mathbf{E}})^2\rangle + 2\frac{\partial^2\tilde{\sigma}_V}{\hbar\,\partial\Omega\partial\epsilon_{23}}\langle(\hat{\epsilon}\cdot\hat{\mathbf{p}})^2(\vec{\mu}_*\cdot\vec{\mathbf{E}})(\vec{\mu}_{23}\cdot\vec{\mathbf{E}})\rangle + \frac{\partial^2\tilde{\sigma}_V}{\partial\epsilon_{23}^2}\langle(\hat{\epsilon}\cdot\hat{\mathbf{p}})^2(\vec{\mu}_{23}\cdot\vec{\mathbf{E}})^2\rangle. \quad (37)$$

Here $\hat{\epsilon}$ is the polarization vector of the absorbed light, $\hat{\mathbf{p}}$ is the unit vector parallel to the transition dipole, $\vec{\mu}_*$ is the difference dipole between the ground state and P^*, and $\vec{\mu}_{23}$ is the difference dipole between P^+B^- and P^*.

To obtain an indication of whether virtual absorption into P^+B^- can have a serious effect on the Stark spectrum, we assume that the P^+B^- dipole is given by the macrocycle distance, $|\vec{\mu}_{23}| \simeq 50$ D. The Stark spectrum of the P band has been used (31, 32, 52) to determine $|\vec{\mu}_*| \simeq 6.5$–$7.0\ \mathrm{D}/f$ at 77 K. Assuming for now that this determination was not significantly affected by the Stark effect on virtual absorption, it appears that the difference moments may differ by almost an order of magnitude. We saw earlier in this section that the strength of the virtual absorption may be a few percent of that of the absorption into P^*. Assuming that the angular factors and energy differentiations do not alter the relative order of magnitude of the terms, we see that the last term (due to virtual absorption) may be comparable to or even larger than the first term (due to absorption into P^*). The location of these two Stark bands in the spectrum may be quite different, however. The virtual absorption can therefore have a serious effect on the deductions one draws from the Stark spectrum.

The shape of the virtual contributions to the Stark spectrum can potentially differ greatly from the second, first, or zeroth derivatives that are commonly used to interpret such spectra. The first term is proportional to the second derivative of the absorption spectrum. The other two terms, however, are not related to any derivatives of the absorption spectrum; the differentiation with respect to ϵ_{23} in general allows them to be completely unrelated functions of Ω. The similarity between the second derivative and Stark effect of the P band (31, 32, 52) then suggests that any peaks due to virtual absorption into P^+B^- are somewhere else in the spectrum. This in turn implies that the value quoted above for the difference dipole $|\vec{\mu}_*|$ between P and P^* has not been perturbed significantly by the virtual absorption Stark effect.

If the Stark effect could be sufficiently well understood, including other effects such as polarizability changes, it is conceivable that it could be used to place an upper bound on the electron transfer matrix element of the first charge transfer transition in the reaction center. Some of the strong deviations from a second-derivative shape seen outside the P band may be due to virtual absorption into a charge-transfer state, and could be the subject of future experimental and modeling efforts.

SUMMARY

We have examined some experiments on the primary charge separation in terms of virtual and two-step electron transfer. The weak energy gap and temperature dependences of the observed rate constant could be generically achieved in the presence of coupling to high-frequency vibrational modes, providing the energy gaps are in the inverted region. This robustness of an experimen-

tal feature with respect to the many parameters of the model allows us to simplify the parameter space we need to consider. Nonetheless, we have not been able to conclusively deduce from the available experimental data whether virtual transfer makes a significant contribution to the primary charge separation. The Stark fluorescence anisotropy data, indicative of virtual transfer, allow an interpretation in terms of two-step transfer within a plausible value for the intermediate state energy range over which the virtual rate varies appreciably.

In the hopes of determining the mechanism of the primary separation, we have suggested a two-pulse excitation experiment that distinguishes two-step from virtual or direct transfer, and discussed the associated problems and their potential solutions. It is certainly conceivable that, together with the body of data already accumulated, it will be possible to determine the contributions of virtual, two-step, and direct transfer to the primary charge separation.

We considered absorption into P^+B^- virtually through P^* and found that its peak cross-section is likely to be much smaller than that of absorption into P^*. However, the band can be centered at a different frequency, so this virtual transition could conceivably contribute to the ground state absorption spectrum and affect the kinetics after excitation. Absorption into P^+B^- can also have an appreciable effect on both the size and shape of the Stark absorption spectrum. If the center of this band were known, it might be possible to use the Stark absorption data to place an upper bound on the electron transfer matrix element connecting P^* with P^+B^-. Models used to fit other experimental data predict the parameters of this band, so experimental investigations in this direction have a hope of measuring one of the most important quantities relating to the primary charge separation.

APPENDIX

Extraction of the rank 0 tensor component

In our discussion of the Stark fluorescence anisotropy data, we use the fact that

$$\langle(\hat{\mu}_{12}\cdot\hat{\mathbf{E}})(\hat{\mu}_{23}\cdot\hat{\mathbf{E}})(\hat{\mathbf{e}}\cdot\hat{\mathbf{p}})^2\rangle = {}^1/_9\hat{\mu}_{12}\cdot\hat{\mu}_{23} + {}^1/_5[(\hat{\mu}_{12}\cdot\hat{\mathbf{p}})(\hat{\mu}_{23}\cdot\hat{\mathbf{p}}) - {}^1/_3\hat{\mu}_{12}\cdot\hat{\mu}_{23}][(\hat{\mathbf{E}}\cdot\hat{\mathbf{e}})^2 - {}^1/_3], \quad (38)$$

where the angled brackets denote an orientational average. We now prove this.

For brevity of notation, let $\vec{\mathbf{u}} = \hat{\mathbf{p}}$, $\vec{\mathbf{v}} = \vec{\mu}_{12}$, and $\vec{\mathbf{w}} = \vec{\mu}_{23}$. Let the Cartesian components of a vector $\vec{\mathbf{v}}$ be denoted by v_α, where $\alpha = 1, 2, 3$, and adopt the Einstein summation convention for repeated indices. It will suffice to show that

$$\langle u_\alpha u_\beta v_\gamma w_\delta\rangle = {}^1/_9u^2\vec{\mathbf{v}}\cdot\vec{\mathbf{w}}\delta_{\alpha\beta}\delta_{\gamma\delta} + {}^1/_5[{}^1/_2(\delta_{\alpha\gamma}\delta_{\beta\delta} + \delta_{\alpha\delta}\delta_{\beta\gamma}) - {}^1/_3\delta_{\alpha\beta}\delta_{\gamma\delta}] \times [(\vec{\mathbf{u}}\cdot\vec{\mathbf{v}})(\vec{\mathbf{u}}\cdot\vec{\mathbf{w}}) - {}^1/_3u^2\vec{\mathbf{v}}\cdot\vec{\mathbf{w}}]. \quad (39)$$

To do this, we remember that only spherical tensors of rank 0 survive a spherical orientational average. We must therefore find the rank 0 piece of this four-index object. We break the problem up by decomposing the two-index objects $u_\alpha u_\beta$ and $v_\gamma w_\delta$ into their spherical tensor components. We have

$$u_\alpha u_\beta = (u_\alpha u_\beta - {}^1/_3u^2\delta_{\alpha\beta}) + {}^1/_3u^2\delta_{\alpha\beta}. \quad (40)$$

In terms of the ranks of the spherical tensor components, this is of the form $\mathbf{2}\oplus\mathbf{0}$. Similarly,

$$v_\gamma w_\delta = [{}^1/_2(v_\gamma w_\delta + v_\delta w_\gamma) - {}^1/_3\vec{\mathbf{v}}\cdot\vec{\mathbf{w}}\delta_{\gamma\delta}] + {}^1/_2(v_\gamma w_\delta - v_\delta w_\gamma) + {}^1/_3\vec{\mathbf{v}}\cdot\vec{\mathbf{w}}\delta_{\gamma\delta}. \quad (41)$$

This is of the form $\mathbf{2}\oplus\mathbf{1}\oplus\mathbf{0}$.

By the same rules used in the addition of angular momenta in quantum mechanics (53), the outer product of two spherical tensors can be decomposed into tensors of only certain ranks:

$$\mathcal{D}^{(j_1)}\otimes\mathcal{D}^{(j_2)} = \sum_{j=|j_1-j_2|}^{j_1+j_2}\mathcal{D}^{(j)}. \quad (42)$$

This is a property of the irreducible representations of the rotation group in three-dimensional space. Therefore, the rank 0 piece of the product consists of only the $\mathbf{0}\otimes\mathbf{0}$ product plus the rank 0 piece of the $\mathbf{2}\otimes\mathbf{2}$ product. This last piece can be calculated if we think of each traceless symmetric rank 2 tensor as a five-component vector with one index corresponding to the pair of Cartesian indices $(\alpha\beta)$. The $\mathbf{2}\otimes\mathbf{2}$ object with four Cartesian indices we are considering then becomes the dyadic product of two such vectors, and its rank 0 component is just one-fifth its trace multiplied by the appropriate 5×5 identity matrix. The trace is easily calculated by contracting the index $(\alpha\beta)$ with the index $(\gamma\delta)$. We need to identify the 5×5 identity matrix. The obvious starting point is $\delta_{\alpha\gamma}\delta_{\beta\delta}$. This must be modified, however, because it is going to act in the space of traceless symmetric 3×3 matrices and must share those properties. To insure tracelessness upon contraction between α and β and also between γ and δ, we make the replacement

$$\delta_{\alpha\gamma}\delta_{\beta\delta} \rightarrow \delta_{\alpha\gamma}\delta_{\beta\delta} - {}^1/_3\delta_{\alpha\beta}\delta_{\gamma\delta}. \quad (43)$$

It must also be symmetric between α and β and between γ and δ. Symmetrizing over both these pairs of indices finally gives

$$I^{5\times5}_{\alpha\beta,\gamma\delta} = {}^1/_2(\delta_{\alpha\gamma}\delta_{\beta\delta} + \delta_{\beta\gamma}\delta_{\alpha\delta}) - {}^1/_3\delta_{\alpha\beta}\delta_{\gamma\delta}. \quad (44)$$

Contracting between the rank 2 tensor indices $(\alpha\beta)$ and $(\gamma\delta)$ gives the value 5, as expected. Putting these pieces together and expressing the quantity of interest as

$$\langle(\hat{\mu}_{12}\cdot\hat{\mathbf{E}})(\hat{\mu}_{23}\cdot\hat{\mathbf{E}})(\hat{\mathbf{e}}\cdot\hat{\mathbf{p}})^2\rangle = e_\alpha e_\beta E_\gamma E_\delta\langle p_\alpha p_\beta\mu_{12\gamma}\mu_{23\delta}\rangle \quad (45)$$

gives the desired result. Similar methods could be used to compute the Stark fluorescence change at higher powers of the electric field.

We thank S. Franzen for helpful conversations.

This work was funded in part by a University of California Regents Fellowship and a National Institutes of Health National Research Service Award (to J. S. Joseph), and a National Science Foundation Presidential Young Investigator Award (to W. Bialek), supplemented by funds from Cray Research Inc., Sun Microsystems, and the NEC Research Institute.

Received for publication 2 December 1991 and in final form 7 April 1992.

References

1. Joseph, J. S., and W. Bialek. 1988. Intermediate states in photosynthetic electron transfer. *Biophys. J.* 53:613*a*. (Abstr.)
2. Joseph, J. S., and W. Bialek. 1989. Virtual intermediates in photosynthetic electron transfer. *Biophys. J.* 55:184*a*. (Abstr.)
3. Franzen, S., R. F. Goldstein, and S. G. Boxer. 1990. Electric field modulation of electron transfer reaction rates in isotropic systems: long distance charge recombination in photosynthetic reaction centers. *J. Phys. Chem.* 94:5135–5149.
4. Martin, J.-L., J. Breton, A. J. Hoff, A. Migus, and A. Antonetti. 1986. Femtosecond spectroscopy of electron transfer in the reaction center of the photosynthetic bacterium *Rhodopseudomonas sphaeroides* R-26: direct electron transfer from the dimeric bacteriochlorophyll primary donor to the bacteriopheophytin acceptor with a time constant of 2.8 ± 0.2 psec. *Proc. Natl. Acad. Sci. USA.* 83:957–961.
5. Breton, J., J.-L. Martin, A. Migus, A. Antonetti, and A. Orszag. 1986. Femtosecond spectroscopy of excitation energy transfer and initial charge separation in the reaction center of the photosynthetic bacterium *Rhodopseudomonas viridis. Proc. Natl. Acad. Sci. USA.* 83:5121–5125.
6. Breton, J., J.-L. Martin, J. Petrich, A. Migus, and A. Antonetti. 1986. The absence of a spectroscopically resolved intermediate state P^+B^- in bacterial photosynthesis. *FEBS (Fed. Eur. Biochem. Soc.) Lett.* 209:37–43.
7. Lockhart, D. J., R. F. Goldstein, and S. G. Boxer. 1988. Structure-based analysis of the initial electron transfer step in bacterial photosynthesis: electric field induced fluorescence anisotropy. *J. Chem. Phys.* 89:1408–1415.
8. Holzapfel, W., U. Finkele, W. Kaiser, D. Oesterhelt, H. Scheer, H. U. Stilz, and W. Zinth. 1989. Observation of a bacteriochlorophyll anion radical during the primary charge separation in a reaction center. *Chem. Phys. Lett.* 160:1–7.
9. Holzapfel, W., U. Finkele, W. Kaiser, D. Oesterhelt, H. Scheer, H. U. Stilz, and W. Zinth. 1990. Initial electron-transfer in the reaction center from *Rhodobacter sphaeroides. Proc. Natl. Acad. Sci. USA.* 87:5168–5172.
10. Kirmaier, C., and D. Holten. 1991. An assessment of the mechanism of initial electron transfer in bacterial reaction centers. *Biochemistry.* 30:609–613.
11. Martin, J.-L., J. Breton, J. C. Lambry, and G. Fleming. 1987. The primary electron transfer in photosynthetic purple bacteria: long range electron transfer in the femtosecond domain at low temperature. *In* The Photosynthetic Bacterial Reaction Center: Structure and Dynamics. NATO ASI Series. J. Breton and A. Vermeglio, editors. Plenum Publishing Corp., New York.
12. Joseph, J. S., W. Bruno, and W. Bialek. 1991. Bleaching of the bacteriochlorophyll monomer band: can absorption kinetic distinguish virtual from two-step electron transfer in bacterial photosynthesis? *J. Phys. Chem.* 95:6242–6247.
13. Joseph, J. S. 1991. Models of photosynthetic electron transfer. Ph.D. thesis. University of California at Berkeley, Berkeley, CA.
14. Deleted in proof.
15. Vos, M. H., J.-C. Lambry, S. J. Robles, D. C. Youvan, J. Breton, and J.-L. Martin. 1991. Direct observation of vibrational coherence in bacterial reaction centers using femtosecond absorption spectroscopy. *Proc. Natl. Acad. Sci. USA.* 88:8885–8889.
16. Hu, Y., and S. Mukamel. 1989. Tunneling versus sequential long-range electron transfer: analogy with pump-probe spectroscopy. *J. Chem. Phys.* 91:6973–6988.
17. Bialek, W., W. J. Bruno, J. S. Joseph, and J. N. Onuchic. 1989. Quantum and classical dynamics in biochemical systems. *Photosynth. Res.* 22:15–27.
18. Higasi, K., H. Baba, and A. Rembaum. 1965. Quantum Organic Chemistry. Interscience Publishers, New York.
19. Gunner, M. R., D. E. Robertson, and P. L. Dutton. 1986. Kinetic studies on the reaction center protein from *Rhodopseudomonas sphaeroides:* the temperature and free energy dependence of electron transfer between various quinones in the Q_A site and the oxidized bacteriochlorophyll dimer. *J. Phys. Chem.* 90:3783–3795.
20. Warshel, A., Z. T. Chu, and W. W. Parson. 1989. Dispersed polaron simulations of electron transfer in photosynthetic reaction centers. *Science (Wash., DC).* 246:112–116.
21. Chu, Z. T., A. Warshel, and W. W. Parson. 1989. Microscopic simulation of quantum dynamics and nuclear tunneling in bacterial reaction centers. *Photosynth. Res.* 22:39–46.
22. Onuchic, J. N., R. F. Goldstein, and W. Bialek. 1990. Biomolecular dynamics: quantum or classical? Results for photosynthetic electron transfer. *In* Perspectives in Photosynthesis. J. Jortner and B. Pullman, editors. D. Reidel Publishing Co., Dordrecht, Holland.
23. Onuchic, J. N. 1987. Effect of friction on electron transfer: the two reaction coordinate case. *J. Chem. Phys.* 86:3925–3943.
24. Closs, G. L., and J. R. Miller. 1988. Intramolecular long-distance electron transfer in organic molecules. *Science (Wash. DC).* 240:440–447.
25. Lockhart, D. J., and S. G. Boxer. 1988. Electric field modulation of the fluorescence from *Rhodobacter sphaeroides* reaction centers. *Chem. Phys. Lett.* 144:243–250.
26. Boxer, S. G., D. J. Lockhart, C. Kirmaier, and D. Holten. 1990. Mechanism of charge separation in photosynthetic reaction centers: electric field effects on the initial electron transfer kinetics. *In* Perspectives in Photosynthesis. J. Jortner and B. Pullman, editors. D. Reidel Publishing Co., Dordrecht, Holland.
27. Bixon, M., and J. Jortner. 1988. Electric field effects on the primary charge separation in bacterial photosynthesis. *J. Phys. Chem.* 92:7148–7156.
28. Creighton, S., J.-K. Hwang, and A. Warshel. 1988. Simulating the dynamics of the primary charge separation process in bacterial photosynthesis. *Biochemistry.* 27:774–781.
29. Lockhart, D. J., S. L. Hammes, S. Franzen, and S. G. Boxer. 1991. Electric field effects on emission line shapes when electron transfer competes with emission: an example from photosynthetic reaction centers. *J. Phys. Chem.* 95:2217–2226.
30. Böttcher, C. J. F. 1973. Theory of Electric Polarization. Vol. 1. Elsevier Science Publishing Co. Inc., New York.
31. Lösche, M., G. Feher, and M. Y. Okamura. 1987. The Stark effect in reaction centers from *Rhodobacter sphaeroides* R-26 and Rhodopseudomonas viridis. *Proc. Natl. Acad. Sci. USA.* 84:7537–7541.
32. Lockhart, D. J., and S. G. Boxer. 1987. Magnitude and direction of the change in dipole moment associated with excitation of the primary electron donor in *Rhodobacter sphaeroides* reaction centers. *Biochemistry.* 26:664–668.
33. Liptay, W., and J. Czekalla. 1960. Die Bestimmung von absoluten Übergangsmomentrichtungen und von Dipolmomenten angeregter Molekülen aus Messungen des elektrischen Dichroismus. I. Theorie. *Z. Naturforsch.* 15a:1072–1079.
34. Deisenhofer, J., O. Epp, K. Miki, R. Huber, and H. Michel. 1984. X-ray structure analysis of a membrane protein complex: electron density map at 3 Å resolution and a model of the chromophores of the photosynthetic reaction center from *Rhodopseudomonas viridis.* J. Mol. Biol. 180:385–398.
35. Deisenhofer, J., O. Epp, K. Miki, R. Huber, and H. Michel. 1985. Structure of the protein subunits in the photosynthetic reaction

center of *Rhodopseudomonas viridis* at 3 Å resolution. *Nature (Lond.)* 318:618–624.

36. Allen, J. P., G. Feher, T. O. Yeates, H. Komiya, and D. C. Rees. 1987. Structure of the reaction center from *Rhodobacter sphaeroides* R-26: The cofactors. *Proc. Natl. Acad. Sci. USA.* 84:5730–5734.
37. Zinth, W., M. Sander, J. Dobler, and W. Kaiser. 1985. Single crystals from reaction centers of *Rhodopseudomonas viridis* studied by polarized light. *In* Antennas and Reaction Centers of Photosynthetic Bacteria. M. E. Michel-Beyerle, editor. Springer-Verlag, Berlin.
38. Lockhart, D. J., C. Kirmaier, D. Holten, and S. G. Boxer. 1990. Electric field effects on the initial electron-transfer kinetics in bacterial photosynthetic reaction centers. *J. Phys. Chem.* 94:6987–6995.
39. Fleming, G. R., J.-L. Martin, and J. Breton. 1988. Rates of primary electron transfer in photosynthetic reaction centres and their mechanistic implications. *Nature (Lond.).* 333:190–192.
40. Holten, D., C. Hoganson, M. W. Windsor, C. C. Schenck, W. W. Parson, A. Migus, R. L. Fork, and C. V. Shank. 1980. Subpicosecond and picosecond studies of electron transfer intermediates in *Rhodopseudomonas sphaeroides* reaction centers. *Biochim. Biophys. Acta.* 592:461–477.
41. Kirmaier, C., D. Holten, and W. W. Parson. 1985. Temperature and detection-wavelength dependence of the picosecond electron-transfer kinetics measured in *Rhodopseudomonas sphaeroides* reaction centers. Resolution of new spectral and kinetic components in the primary charge-separation process. *Biochim. Biophys. Acta.* 810:33–48.
42. Knox, W. H. 1988. Femtosecond optical pulse amplification. *IEEE (Inst. Electr. Electron. Eng.) J. Quant. Electron.* 24:388–397.
43. Bialek, W. 1983. Quantum effects in the dynamics of biological systems. Ph.D. thesis. University of California at Berkeley, Berkeley, CA.
44. Feher, G. 1987. The Stark effect in photosynthetic reaction centers from *Rhodobacter sphaeroides* R-26, *Rhodopseudomonas viridis* and the D_1D_2 complex of photosystem II from spinach. *In* The Photosynthetic Bacterial Reaction Center: Structure and Dynamics. NATO ASI Series. J. Breton and A. Vermeglio, editors. Plenum Publishing Corp., New York.
45. Boxer, S. G., T. R. Middendorf, and D. J. Lockhart. 1986. Reversible photochemical hole-burning in *Rhodopseudomonas viridis* reaction centers. *FEBS (Fed. Eur. Biochem. Soc.) Lett.* 200:237–241.
46. Meech, S. R., A. J. Hoff, and D. A. Wiersma. 1986. Role of charge-transfer states in bacterial photosynthesis. *Proc. Natl. Acad. Sci. USA.* 83:9464–9468.
47. Vos, M. H., J.-C. Lambry, S. L. Robles, D. C. Youvan, J. Breton, and J.-L. Martin. 1992. Femtosecond spectral evolution of the excited state of bacterial reaction centers at 10*K*. *Proc. Natl. Acad. Sci. USA.* 89:613–617.
48. Kirmaier, C., E. J. Bylina, D. C. Youvan, and D. Holten. 1989. Subpicosecond formation of the intradimer charge transfer state [$BChl^{+}_{LP}BPh^{-}_{MP}$] in reaction centers from the $His^{M200} \rightarrow$ Leu mutant of *Rhodobacter capsulatas. Chem. Phys. Lett.* 159:251–257.
49. McDowell, L. M., C. Kirmaier, and D. Holten. 1990. Charge transfer and charge resonance states of the primary electron donor in wild-type and mutant bacterial reaction centers. *Biochim. Biophys. Acta.* 1020:239–246.
50. Sakurai, J. J. 1967. Advanced Quantum Mechanics. Benjamin/Cummings Publishing Co., Menlo Park, CA.
51. Kharkats, Y. I., A. K. Madumarov, and M. A. Vorotyntsev. 1974. Application of the density matrix method in the quantum mechanical calculation of the bridge-assisted electron transfer probability in polar media. *J. Chem. Soc., Farad. Trans. 2.* 70:1578–1590.
52. Lockhart, D. J., and S. G. Boxer. 1988. Stark effect spectroscopy of *Rhodobacter sphaeroides* and *Rhodopseudomonas viridis* reaction centers. *Proc. Natl. Acad. Sci. USA.* 85:107–111.
53. Wigner, E. P. 1959. Group Theory and its Application to the Quantum Mechanics of Atomic Spectra. Academic Press, New York.